D-Cycloserine destruction by alanine racemase and the limit of irreversible inhibition

Cesira de Chiara[1], **Miha Homšak**[1,2], **Gareth A. Prosser**[1,#], **Holly L. Douglas**[1], **Acely Garza-Garcia**[1], **Geoff Kelly**[3], **Andrew G. Purkiss**[4], **Edward W. Tate**[2,5], **Luiz Pedro S. de Carvalho**[1,*]

[1]Mycobacterial Metabolism and Antibiotic Research Laboratory, The Francis Crick Institute, 1 Midland Road, NW1 1AT, London, UK

[2]Department of Chemistry, Imperial College London, The Molecular Sciences Research Hub, 80 Wood Lane, W12 0BZ, London, UK

[3]MRC Biomedical NMR Centre, The Francis Crick Institute, 1 Midland Road, NW1 1AT, London, UK

[4]Structural Biology Science Technology Platform, The Francis Crick Institute, 1 Midland Road, NW1 1AT, London, UK

[5]Chemical Biology Satellite Laboratory, The Francis Crick Institute, 1 Midland Road, NW1 1AT, London, UK

Summary

The broad-spectrum antibiotic D-cycloserine (DCS) is a key component of regimens used to treat multi- and extensively drug-resistant tuberculosis. DCS, a structural analogue of D-alanine, binds to and inactivates two essential enzymes involved in peptidoglycan biosynthesis, alanine racemase (Alr) and D-Ala:D-Ala ligase. Inactivation of Alr is thought to proceed via a mechanism-based irreversible route, forming an adduct with the pyridoxal 5'-phosphate cofactor, leading to bacterial death. Inconsistent with this hypothesis, *Mycobacterium tuberculosis* Alr activity can be detected after exposure to clinically relevant DCS concentrations. To address this paradox, we investigated the chemical mechanism of Alr inhibition by DCS. Inhibition of *M. tuberculosis* Alr and other Alrs is reversible, mechanistically revealed by a previously unidentified DCS-adduct hydrolysis.

*Correspondence to: Luiz P. S. de Carvalho. luiz.carvalho@crick.ac.uk.
#Current address: Cancer Research UK Manchester Institute, The University of Manchester, Alderley Park, SK10 4TG.

Dissociation and subsequent rearrangement to a stable substituted oxime explains Alr reactivation in the cellular milieu. This knowledge provides a novel route for discovery of improved Alr inhibitors against *M. tuberculosis* and other bacteria.

D-Cycloserine (DCS) is an antibiotic produced by *Streptomyces lavendulae* and *S. garyphalus* simultaneously discovered by Merck and Lilly in 1955[1]. DCS is a broad-spectrum antibacterial agent currently used as the cornerstone drug in regimens employed in the therapy of multidrug (MDR) and extensively drug (XDR) resistant tuberculosis (TB)[2]. WHO estimates that approximately 450,000 cases of tuberculosis in 2017 were due to MDR and XDR strains infections. In addition, DCS was approved by the FDA in 2011 for the treatment of refractory enteric infections caused by *Clostridium difficile*, indicating a renewed interest in its antibacterial activities beyond tuberculosis.

DCS is a D-Ala structural analogue and targets two essential enzymes of the cell wall peptidoglycan biosynthetic pathway, alanine racemase (Alr) and D-Ala:D-Ala-ligase (Ddl)[3]. Despite numerous studies on the mechanism of action of DCS over six decades, unexpected findings are emerging. For example, Ddl inhibition by DCS has been shown to proceed via formation of a phosphorylated DCS species, instead of simple reversible inhibition. Formation of this DCS-phosphate species is analogous to the physiological reaction of Ddl[4], where D-Ala-phosphate precedes dipeptide formation[5].

Alr enzymes are pyridoxal 5'-phosphate (PLP)-dependent enzymes, in which the cofactor is covalently attached to an active-site lysine side chain via an internal aldimine linkage (**1**; Fig. 1a). According to the currently proposed mechanism of inactivation (Fig. 1a)[6], DCS (**3**) binds to the Ala site, attacks PLP, displaces the lysine side chain (**2**) and forms an external aldimine linkage to PLP (**4**). This external aldimine (hereafter indicated as 'the aldimine') is converted in a multi-step reaction catalysed by general acids/bases into a stable pyridoxamine 5′-phosphate-like (PMP-like) isoxazole derivative **6** (hereafter indicated as 'the isoxazole') (Fig. 1a), which is believed to be an irreversible inhibitor. Noticeably, the aldimine **4**, the intermediate ketimine **5** and the final isoxazole **6** are structural isomers, having the same empirical formula in their fully uncharged state ($C_{11}H_{14}N_3O_7P$).

The currently proposed inactivation mechanism, known as the 'aromatization' mechanism, was originally inferred in 1998 from studies on cycloserine inactivation of distinct PLP-enzymes, γ-aminobutyric acid aminotransferase (GABA-AT)[7] and D-amino acid aminotransferase (DAAT)[8]. These studies led to a proposed reversible connection between the final isoxazole and the other intermediates for the analogous inactivation of GABA-AT[7], as well as a proposal that formation of the final isoxazole during inactivation of DAAT was irreversible, likely due to the expected thermodynamic stability of the aromatic ring[8]. Based on this work, irreversible formation of the isoxazole was proposed/assumed for all Alr enzymes[6] (Fig. 1a). Since then, a derivative representing the expected isoxazole has been systematically fitted into the positive electron density map of several DCS-inhibited Alr orthologues solved by X-ray crystallography[6,9–13]. Interestingly, no structures of DCS-inhibited MtAlr have been determined, in spite of DCS having been used for over 50 years in the therapy of drug resistant TB and the crystal structure of the active enzyme being solved in 2005[14].

In 2013, we demonstrated that Alr is not fully inhibited in *Mycobacterium tuberculosis* treated with DCS[15]. The same conclusion was subsequently reached by others[16]. More recently, we showed that Alr levels are unchanged upon treatment with DCS, indicating that lack of full inhibition is not caused by newly synthesised Alr[17]. Therefore, incomplete inhibition is incompatible with the irreversible inhibition mechanism (Fig. 1a), as all enzyme molecules should be inhibited at inhibitor concentrations greater than the enzyme concentration[18].

Given this paradox and the lack of mechanistic and structural data on the inhibition of *Mycobacterium tuberculosis* Alr (MtAlr) by DCS, we undertook a systematic analysis of the inhibition mechanism employing inhibition kinetics, synthetic organic chemistry, mass spectrometry, NMR, UV/Vis, fluorescence and circular dichroism (CD) spectroscopy, model reactions, and X-ray crystallography. Our results reveal the existence of a previously unrecognized pathway involving DCS-ring opening and reactivation of MtAlr. This parallel pathway is a general feature observed in several Alr enzymes.

Results

DCS inactivation of MtAlr leads to distinct products

The structures of six wild-type orthologue Alrs in both the active and DCS-inhibited states (*B. stearothermophilus*[6], *S. lavendulae*[9], *E. coli*[10], *E. faecalis*[11], *C. difficile*[12] and *S. coelicolor*[13]) have been reported. Alrs are functional homodimers in which the two monomers are arranged in a head to tail fashion and each active site is formed by residues contributed by the two distinct chains. Among these are two catalytic residues, Lys44 and Tyr273' (numbering refers to MtAlr). The structures of all the available DCS-inhibited Alrs show in the active site a covalent adduct formed by DCS and PLP. Consistent with the assumed complete and irreversible mechanism of inhibition, two identical molecules representing the isoxazole (**6**; Fig. 1a) have been modelled into the positive density of both sites, in all structures.

To provide the missing structural information for our mechanistic investigation, we determined the structure of the DCS-inhibited MtAlr at 1.56 Å by growing crystals of the DCS-inhibited MtAlr (Fig. 1b). The structure was solved by molecular replacement using the available coordinates of the active MtAlr (1XFC) (Supplementary Table 1). The active MtAlr structure presented features of an asymmetric dimer with two loops contributing to active site A (Val176-Lys180 from chain A and Arg266'-Pro280' from chain B which includes the catalytic Tyr273') missing from the 1XFC coordinates. Positive electron density was present for these loops in the post-molecular replacement map of DCS-inactivated MtAlr (this study). Although this density was less well-defined than for site B, fitting of all the missing residues in site A was possible. The density for the adduct formed by PLP and the antibiotic is well-defined in both active sites (Fig. 1b,c).

However, there are clear differences in the antibiotic ring density, suggestive of distinct products in the two sites. Whereas the planar density in site B is indicative of a molecule with its α carbon in a sp^2 hybridization state (Fig. 1c), the density in site A indicates that the antibiotic ring is at an angle with the axes of the N-Cα bond, suggesting that at least a

fraction of the molecules are showing sp^3 hybridization for Cα (tetrahedral geometry) (Fig. 1b). Additionally, weaker density is observed in active site A (Fig. 1b) for the Cβ atom from the antibiotic ring likely due to the presence of chemical heterogeneity. In agreement with these features, while the isoxazole (**6**; Fig. 1a,c) is satisfactorily fitted in site B as the sole species, a mixture of isoxazole (occupancy 0.96) and aldimine (0.04) (**4**; Fig. 1a,b) is required in order to fulfil the positive density in site A. These results are inconsistent with the current model (Fig. 1a), where, at equilibrium, both active sites should be fully inhibited by isoxazole adducts.

DCS appears to act as an irreversible inhibitor

The inactivation of Alrs by DCS has historically been monitored by UV/Vis spectroscopy, following the disappearance of the initial λ_{max} ~430 nm absorbance band and the formation of a product band at λ_{max} ~320 nm[19]. According to the currently proposed mechanism[6] (Fig. 1a), the internal and external aldimine formed by MtAlr with DCS (**1** and **4**), both characterized by a tetrahedral Cα carbon (sp^3 hybridization), share identical absorbance at λ_{max} 425 nm (Fig. 1d). In contrast, the transient ketimine intermediate and the final PMP-like isoxazole, both with a planar Cα carbon (sp^2 hybridization) (**5** and **6**), share the absorbance of the newly formed band at λ_{max} 318 nm (Fig. 1d).

Inactivation kinetics experiments reveal that both MtAlr and *E. coli* Alr (EcAlr) are inhibited by DCS with similar kinetics (Fig. 1e), with the former (k_{inact}/K_i = 19.3 M^{-1} s^{-1}) being inhibited approximately twice as fast as the latter (k_{inact}/K_i = 8.6 M^{-1}s^{-1}). EcAlr was chosen as a control, as irreversible inhibition has been documented[20]. In contrast, *S. lavendulae* Alr (SlAlr) appears to be substantially less inhibited, confirming the hypothesis that it is "resistant" to DCS produced by the organism[9,21]. Inactivation rates of MtAlr at low inhibitor concentration indicate that DCS behaves as a typical irreversible inhibitor, with a linear fitting of the data intersecting the y-axis at zero (Fig. 1f).

Removal of excess DCS reveals formation of active MtAlr

Next, we sought to test whether reactivation of MtAlr would take place following extensive dialysis or ultrafiltration. Alr enzymes were initially incubated with DCS to obtain the inhibited form and then dialysed. We tested the residual activity of the enzyme by employing the coupled enzymatic assay and by directly monitoring the conversion of L-Ala into D-Ala by CD. Both techniques consistently showed the enzyme retaining approximately 3-5% of activity compared to uninhibited control without any pre-incubation with exogenous PLP. Indeed, MtAlr appeared to consistently retain 3-5% of activity after dialysis while only 0.3% activity was recovered with EcAlr (Fig. 2a). The activity retained by MtAlr showed a slight increase when the protein was pre-incubated with additional PLP (Fig. 2a, inset).

MtAlr readily incorporates deuterium into DCS

We next investigated whether mechanistic differences between MtAlr and EcAlr inactivation by DCS could be observed in D$_2$O-containing buffer, given the number of proton transfers taking place in the inactivation mechanism. Liquid chromatography coupled to high resolution mass spectrometry (LC-MS) was employed for these experiments. Unexpectedly, MtAlr leads to a time-dependent increase in the mass of DCS by 1 AMU, DCS+1 (m/z =

103.0502 to $m/z = 104.0565$), when incubated in D_2O-containing buffer for 2 hours, leading to approximately 50% deuteration of DCS under the experimental conditions (Fig. 2b). This increase in mass was not observed in H_2O-containing buffer or in the presence of heat-inactivated MtAlr, and was considerably slower in the presence of EcAlr (Supplementary Fig. 1a). Interestingly, no increase in mass was observed when MtAlr was incubated with L-cycloserine (LCS) in D_2O-containing buffer (Supplementary Fig. 1b).

We then used NMR and CD spectroscopy to assess whether deuterium incorporation was coupled to replacement of a proton in either the α or the β position, and, if in the α position, whether racemization would occur (Fig. 2c and Supplementary Fig. 1c). ^{1}H and ^{13}C NMR experiments confirmed that MtAlr replaces the α proton of DCS with a deuteron. Deuteration of DCS was not observed when MtAlr was heat-inactivated prior to addition to the reaction mixture (Fig. 2d), indicating that deuteration is an enzyme-catalysed reaction. Integration of the NMR signals reveals that ~ 35% of deuteration is observed in this experiment, in agreement with the result obtained by LC-MS (Fig. 2b). As illustrated by Supplementary Fig. 1c, CD measurements confirmed that MtAlr does not catalyse the conversion of DCS to LCS, whereas, as expected, it is able to convert L-Ala into D-Ala. The deuteration of DCS but not LCS is likely due to stereospecific internal return[22]. That is, the general base that abstracts and returns the proton with LCS is monoprotic (Tyr273), while with DCS, a polyprotic base, Lys44, leads to deuteration. Together, these results point to important differences in the chemical mechanism of inhibition between Alr homologues.

Fluorescence reveals a second inactivation product

Given the low discriminatory power of UV/Vis absorbance spectroscopy, we exploited the higher sensitivity and resolution of fluorescence for monitoring DCS binding and MtAlr inactivation. Indeed, fluorescence revealed a more complex ensemble of species than UV/Vis. Following excitation at λ_{max} 434 nm, the internal aldimine **1** of the active enzyme emitted fluorescence at λ_{max} 520 nm (Supplementary Fig. 2a), which was stable for several hours at 37 °C and upon DCS addition decayed within 15 min (Supplementary Fig. 2b).

Unexpectedly, two distinct fluorescent products were formed, one absorbing light at λ_{max} 318 nm and emitting light at 357 nm and the other absorbing at λ_{max} 365 nm and emitting at 454 nm (Fig. 2e and Supplementary Fig. 2c). Band I, corresponding to the only product observed in the UV spectrum, was formed with a rate comparable to the decay of the internal aldimine **1** (Supplementary Fig. 2d), whereas the additional band II increased almost linearly at a substantially lower rate and reached a plateau over ~ 24 h (Supplementary Fig. 2e). Both products are formed in the inactivation reaction of MtAlr over a pH range from 6.5 to 8.5 with lower rate and final concentration for band I at pH 6.5 (Supplementary Fig. 2f). Importantly, the formation of a species giving rise to band II could be observed in all the Alr orthologues tested, including SlAlr, EcAlr and *Bacillus subtilis* Alr (BsAlr), thus suggesting conservation of the mechanism between species (Supplementary Fig. 2g-i). The three additional orthologues were chosen for comparison with MtAlr as they are representative of different polymorphic variants observed in the active site residues throughout the family, i.e. at positions 90, 91, 320 and 323 of MtAlr. Therefore, by comparing MtAlr with the other

homologues we could confidently conclude that what is observed for MtAlr is not unique to this enzyme (Supplementary Fig. 2j).

By testing the enzymatic reaction mixture in a filtration experiment, we established that species I remains tightly bound to the protein, whereas species II is readily and quantitatively removed, likely due to very low affinity for the enzyme (Supplementary Fig. 2k).

The chemical structure of species I and II

Based on the excitation wavelength (λ_{max} 318 nm), band I could be putatively assigned to PMP-like products **5** and/or **6** (Fig. 1a). However, the observed difference of 39 nm between the maximum excitation and emission wavelengths (λ_{max} ~ex 318/em 357 nm) is smaller than that expected at neutral pH. The Stokes shift is usually about 65 nm (λ_{max} ~ex 327/em 392 nm) for PMP or PMP-like derivatives in buffer[23] or, for instance, in PMP-binding aspartate amino transferase (AAT)[24]. This is also the case for the MtAlr internal aldimine **1** bond when reduced with NaBH$_4$ (Supplementary Fig. 3a). To confirm that species I is the isoxazole (**6**), the compound was chemically synthesized (Fig. 3a) and characterised by UV/Vis absorbance, fluorescence, NMR, and LC-MS (Fig. 3b-g and Supplementary Fig. 3b-e). To the best of our knowledge, this is the first report of a successful synthesis of the isoxazole **6** (see Online Methods). Interestingly, our NMR characterization of the synthetic isoxazole revealed that the compound spontaneously tautomerizes to ketimine **5** (Fig. 3a) in buffered solution, as indicated by both the formation of up to ~20% of ketimine after 24 hours at 37 °C (Fig. 3b,c) and the observed H/D exchange of the isoxazole β-proton at room temperature (Fig. 3d). These results indicate that the isoxazole **6** is in relatively fast equilibrium with the ketimine **5** both in solution and on-enzyme, and therefore the isoxazole **6** is not an irreversible, stable adduct.

In spite of the isoxazole excitation wavelength (λ_{max} 329 nm) being similar to the one of band I (λ_{max} 318 nm) of the enzymatic reaction in the same buffer, the compound emits fluorescence at a longer wavelength (λ_{max} 388 nm) than the enzymatic product (λ_{max} 357 nm), matching the larger Stokes shift expected for such compounds around neutral pH[23] (Supplementary Fig. 3c).

To test whether the observed difference in the isoxazole Stokes shift is due to intrinsic differences in the on-enzyme versus in solution environments, apo-MtAlr was prepared by treatment with hydroxylamine followed by dialysis at acidic pH to eliminate the PLP hydroxylamine derivative. The fluorescence spectrum of the reconstituted inhibited enzyme, obtained by treatment of apo-MtAlr with an excess of synthetic isoxazole followed by dialysis for elimination of any free compound **6** (Fig. 3e), matches the spectrum of band I from the enzymatic reaction (Fig. 2e), confirming the identity of the isoxazole. The isoxazole emission wavelength is therefore blue shifted when bound to the enzyme as compared to 'in-solution' (Supplementary Fig. 2c,3c). Based on fluorescence studies of pyridoxamine[25,26] and PMP[23], a blue shift is suggestive of a more basic local pH of the active site pocket, which leads to deprotonation of the pyridine nitrogen. This indicates that the environment of the MtAlr active site affects the protonation state and fluorescence of the isoxazole (Supplementary Fig. 3f). Deprotonation of the pyridine nitrogen in Alrs is also

supported by NMR studies on protonation of internal aldimine in BsAlr[27]. Further evidence supporting the identity of band I as the isoxazole comes from LC-MS, which showed the same retention time and *m/z* for synthetic and enzymatically formed isoxazole (Fig. 3f,g).

The spectroscopic features of band II (Fig. 4a) suggested that this product could be an oxime derivative of PLP, as indicated by the strict resemblance to the fluorescence emission band of the product formed in a model reaction between PLP and DCS. Indeed, the possibility that the reaction of DCS with PLP in buffer could lead to a rapid hydrolysis of the isoxazolidinone ring (**8**) and rearrangement by transaldimination into a substituted oxime **11** (hereafter indicated as 'the oxime'), had been suggested in 1963 based on spectroscopic similarity (Fig. 4a), but never confirmed[28].

To determine the structure of the model reaction product we employed 1D-^{1}H, 1D-^{13}C, ^{1}H-^{13}C, and ^{1}H-^{15}N NMR experiments (Fig. 4c,d and Supplementary Fig. 4a,b). Initial experiments confirmed the formation of the oxime (Fig. 4b; **10** or **11**). By repeating the experiment in a $H_2^{16}O:H_2^{18}O$ (1:1) buffer solution, we could confirm that the final oxime product is linear (Fig. 4b; **11**) rather than cyclic **10**, as hydrolysis causes a split of the DCS carbonyl ^{13}C signal resulting from ^{18}O-isotopic effect (Fig. 4c). The chemical identity of the product of the model reaction **11** and of its counterpart from the enzymatic reaction, i.e. species II, was further supported by LC-MS and collision induced dissociation MS as a substituted oxime (Fig. 4e,f and Supplementary Fig. 4c,d). The formation of **11** in the model reaction was also monitored by fluorescence and LC-MS, showing that the compound is stable to hydrolysis over 120 h (Supplementary Fig. 4e,f).

Isoxazole (6) is not an irreversible inhibitor of MtAlr

The continuous formation of the oxime over ~24 h indicates that the aldimine **4**, the species from which the oxime originates, remains present to some extent in the active site after the isoxazole formation has reached a plateau (Fig. 5a). By comparing the fluorescence intensity of the oxime from the enzymatic reaction with that of a solution of a 'model' compound of known concentration we could estimate the released oxime being in the order of ~3% at the isoxazole plateau and ~10% by 24 h (Fig. 5a). Interestingly, by 24 h the isoxazole fluorescence intensity decreases accordingly by ~5% (Fig. 5a), suggesting conversion of one species into the other, via the reverse reaction from isoxazole **6** to aldimine **4** (Fig. 1a).

The existence of an equilibrium and therefore the reversibility of the inactivation reaction is additionally confirmed by the formation of a new oxime **11** from the aldimine **4**, starting soon after the original oxime has been quantitatively eliminated by ultrafiltration (Fig. 5b). This indicates that at plateau, the enzymatic reaction reaches a pseudo-equilibrium between all species from **1** to **6** (Fig. 1a) rather than irreversibly leading to formation of 100% isoxazole **6**. Finally, further evidence in support of an equilibrium and reversibility is derived from the sample of the isoxazole-inhibited MtAlr reconstituted from apo-MtAlr, which shows the presence of a species emitting fluorescence identical to band II (Fig. 3e).

Altogether, these findings allowed us to present a revised mechanism of Alr inhibition by DCS (Fig. 6) which includes a second path, branching from the aldimine **4** and leading to the formation of the oxime **11**. The revised mechanism, presenting an 'oxime-forming

pathway' alongside a reversible 'isoxazole-forming pathway' is of general relevance as our data show that the oxime formation appears to be conserved across species (Supplementary Fig. 2g-i).

Discussion

Here we present a comprehensive study on the chemical mechanism of Alr inhibition by DCS. Despite the past assumption that DCS causes complete and irreversible inhibition of Alr, incomplete inhibition in cells has been observed[15]. Our mechanistic analysis solves this apparent paradox, highlighting the presence of two key features. First, there is a pseudo-equilibrium between the different species of the inactivation reaction reversibly connecting the isoxazole **6** with the aldimine **4**. Second, we demonstrate the existence of a slower parallel reaction which explains how a proposed irreversible inhibitor can lead to incomplete inhibition in cells[15,29].

The presence of aldimine **4** at equilibrium explains the incomplete inactivation observed in mycobacteria, as it enables the oxime-forming route[28]. Hydrolysis of the isoxazolidinone ring of the aldimine **4** leads to ring opening and subsequent intramolecular transaldimination to generate a stable oxime **11**. As a consequence, a fraction of the active sites, estimated to be up to 10% after 24 h at 37 °C, is left in an 'apo' state and can be reconstituted with free PLP, regenerating active MtAlr. The oxime-forming route is of particular importance for MtAlr inhibition during tuberculosis treatment, as opposed to fast-growing bacteria, in view of the slow doubling time of *Mycobacterium tuberculosis* (~20 h). This oxime-forming route might also represent an underappreciated source for DCS resistance in the biome. Hundreds of polymorphisms exist in *alr* genes, some of which might lead to faster ring opening and Alr re-activation post DCS treatment. In summary, the oxime-forming pathway might be partially responsible for the narrow clinical usefulness of DCS despite its broad spectrum.

The formation of a substituted oxime by DCS treatment of a PLP-dependent enzyme has so far been documented only for aspartate-glutamate transaminase[30] and, to the best of our knowledge, no suggestions of a similar reaction have been reported in literature for any Alrs.

Is the oxime-forming pathway partially or entirely 'off-enzyme'? The first consideration is if the aldimine **4** is released into solution. No dissociation of the aldimine **4** was observed under any experimental condition. This leaves two remaining possibilities: the aldimine **4** is hydrolyzed 'on-enzyme' forming **9**, which upon dissociation rapidly rearranges into an oxime **11**, as confirmed by the NMR experiments on the model compound. Alternatively, the transaldimination reaction converting **9** into **11** occurs 'on-enzyme', with subsequent release of the oxime **11** in solution. The latter proposal cannot be formally excluded, although it appears less likely since steric hindrance generated in the active site during the transaldimination step would be unfavourable. In both cases, similarly to the uptake of PLP, the release of PLP derivatives from the enzyme active site into solution is made possible by the existence of a monomer-dimer equilibrium[31,32]. In the absence of such an equilibrium, no molecule bigger than the substrate could be exchanged in and out of the active site. In summary, the most likely mechanism would involve hydrolysis of **8** in the active site generating **9**, which is released in solution and rapidly re-arranges to oxime **11** (Fig. 6).

The crystal structure of DCS-inhibited MtAlr supports the conclusion of the mechanistic study by showing both external aldimine and isoxazole in one of the sites and confirming the existence of an equilibrium between species. Furthermore, a 0.04 occupancy for the aldimine is in agreement with the persistent/regained 3% activity of inhibited MtAlr, after removal of free DCS. The differences between the products observed in the two active sites are suggestive of genuine structural and functional asymmetry and have been observed before[14].

A comparative analysis of amino acid conservation between MtAlr, EcAlr, SlAlr and BsAlr identified three tightly bound water molecules in the active site within 5 Å of the carbonyl group of DCS, which could participate in DCS hydrolysis (Fig. 1b,c). The closest water at 3.3 Å, hydrogen bonded to the carbonyl oxygen, might contribute to making the carbonyl carbon more electrophilic. A second water, 4.3 Å from the carbonyl carbon, is at ~3.5 Å to His174 and 3.8 Å to Tyr273'. Both residues might be working to deprotonate and activate the water molecule for nucleophilic attack. The third water, at 3.7 Å to the carbonyl, is also at 2.6 Å from Tyr292'. However, pK_a calculations for BsAlr indicate that Tyr292' might be fully protonated[33].

This study reveals that DCS is a slow, yet reversible covalent inhibitor of Alr enzymes. This discovery illustrates the complexity of understanding detailed chemical mechanisms of enzyme inhibitors. The observation that *M. tuberculosis* Alr inhibition was incompatible with complete irreversible inhibition led us to investigate the consensus mechanism. While Alr enzymes from *E. coli* and other fast-growing bacteria are effectively inhibited by DCS, those from *M. tuberculosis* and likely other slow-growing bacteria are not. In this particular case, the slow-growing nature of *M. tuberculosis* might contribute to Alr reactivation.

Few chemical reactions are truly irreversible and caution is advised in evaluating covalent inhibitors that may behave "irreversibly" in the chemically simple *in vitro* conditions and "reversibly" in the more complex *in vivo* milieu. This is particularly important in antibiotic research as bacterial pathogens have growth rates that span several orders of magnitude. Slowing down their growth rate is one of the key mechanisms used by these organisms to avoid antibiotic-induced toxicity.

Online Methods

Protein expression and purification

Recombinant MtAlr was co-expressed with the mycobacterial GroEL homologue Cpn60.2 and E. coli GroES chaperone proteins using the plasmid pTrc60.2-p15a (plasmid pTrc-60.2-GroES) modified in our lab to carry the p15a origin of replication[34,35]. EcAlr, BsAlr and SlAlr were co-expressed with both E. coli GroES and GroEL using the pGro7 plasmid from the Takara kit for co-expression of chaperones with non-mycobacterial enzymes (Takara Bio, Cat.# 3340). All Alrs were expressed in *E. coli* BL21 cells using a pET28a+ plasmid with an amino-terminal cleavable His-tag. After cells harvesting, resuspension in buffer (20 mM TEA pH 7.8, 100 mM NaCl, 20 mM imidazole), lysis by sonication, and centrifugation, Alrs were purified from the supernatant by Ni-NTA affinity chromatography. After cleavage of the His-tag by thrombin overnight at 4 °C, the protein was reapplied to a His-Trap Ni-

NTA column and then further purified from thrombin on a Heparin column equilibrated with 20 mM TEA, 100 mM NaCl, and 100 mM glycine. After concentration, a final purification was performed by gel filtration using a 26/60 Sephadex column. The protein was then concentrated and dialysed against 20 mM sodium phosphate buffer (pH 7.5) containing 150 mM NaCl. The protein concentration was determined by the UV absorbance at 280 nm, using calculated extinction coefficients corrected for the contribution of the internal aldimine to absorbance at the same wavelength.

Preparation of apo MtAlr and reconstitution with synthetic isoxazole—MtAlr at 150 μM treated with 1 mM hydroxylamine was extensively dialysed against 100 mM sodium phosphate buffer pH 5.0 with 0.5 mM hydroxylamine. Apo-MtAlr was then incubated with 130 μM of synthetic isoxazole and extensively dialysed against 20 mM sodium phosphate buffer (pH 7.5) to remove any unbound isoxazole.

LC -MS

H/D exchange experiments—LC-MS analysis was performed on an Agilent 1200 LC system coupled to an Agilent Accurate Mass 6230 ToF. Chromatography was performed using a Cogent Diamond Hydride Type C silica column (150 mm × 2.1 mm; dead volume 315 μl) maintained at 40 °C. The flow rate was 0.4 ml min-1. The mobile phase consisted of 0 min 85 % B; 0-2 min 85 % B; 2-3 min to 80 % B; 3-5 min 80 % B; 5-6 min to 75 % B; 6-7 min 75 % B; 7-8 min to 70 % B; 8-9 min 70 % B; 9-10 min to 50 % B; 10-11 min 50 % B; 11-11.1 min to 20 % B; 11.1-14 min hold at 20 % B. Solvent A consisted of deionized water with 0.2 % acetic acid, and solvent B consisted of acetonitrile and 0.2 % acetic acid.

Dynamic mass axis calibration was achieved by continuous infusion of a reference mass solution using an isocratic pump connected to a multimode ionization source, operated in the positive-ion and negative-ion mode. ESI capillary and fragmentor voltages were set at 3500 V and 100 V, respectively. The nebulizer pressure was set at 40 psi and the nitrogen drying gas flow rate was set at 10 L min-1. The drying gas temperature was maintained at 250 °C. The MS acquisition rate was 1.5 spectra/sec and m/z data ranging from 50-1200 were stored. This instrument routinely enabled accurate mass spectral measurements with an error of less than 5 parts-per-million (ppm), mass resolution ranging from 10,000-25,000 over the m/z range of 121-955 atomic mass units, and a 100,000-fold dynamic range with picomolar sensitivity. Data were collected in the centroid mode in the 4 GHz (extended dynamic range) mode.

Sample preparation for LC-MS analysis of isoxazole and oxime.—The isoxazole and substituted oxime samples from the enzymatic reaction were prepared by treating 200 μM MtAlr with 10 mM DCS in 20 mM potassium phosphate buffer (pH 7.5) and incubating at 37 °C for 24 h in the dark. Ultrafiltration with Vivaspin 10 K cut-off provided a low molecular weight flow through fraction containing oxime at an estimated concentration of 20 μM and an on-filter fraction containing 400 μM MtAlr bound to isoxazole and ~20 μM free oxime. The release of the isoxazole from MtAlr for LC-MS detection could only be achieved by heating of the sample at 65 °C for 30 min prior to LC-MS sample preparation. The oxime sample from the model reaction was prepared by incubating 250 μM PLP with

2.5 mM DCS in 20 mM TEA buffer (pH 7.5) at 37 °C overnight in the dark. The LC-MS samples were prepared by dilution into the LC-MS mobile phase A (see below) followed by centrifugation and collection of the supernatant.

Oxime model and enzymatic reaction products—LC-MS analysis was performed on an Agilent 1290 LC system coupled to an Agilent 6560 Ion Mobility Q-ToF (operated in Q-ToF only mode).

Chromatography was performed using a Waters XBridge Amide column, 3.5 μm, 4.6 x 100 mm maintained at 40 °C. Mobile phase A was 95% 20 mM ammonium hydroxide, 20 mM ammonium acetate, pH 9.0; 5% acetonitrile. Mobile phase B was acetonitrile. Analytes were eluted using a flow rate of 0.4 mL min^{-1} and the following mobile phase gradient: 0 – 5 min, 85 – 60% B; 5 – 16 min, 60% B; 16 – 21 min, 60 – 2 % B; 21 – 26 min, 2 – 85% B. The system was re-equilibrated to initial conditions for six minutes at the end of each run. The injection volume was 10 μL for all standards and samples.

The Q-ToF was operated in positive-ion mode with electrospray ionisation (ESI) using a dual AJS ESI source. Capillary, nozzle and fragmentor voltages were set at 4000 V, 500 V and 350 V respectively. The nebulizer pressure was set at 25 psi and the nitrogen drying gas flow rate was set at 11 L min^{-1}. The drying gas temperature was maintained at 350 °C. The sheath gas temperature and flow rate were 400 °C and 12 L min^{-1}. The collision energy used to acquire the product ion spectrum was 15 eV. Dynamic mass axis calibration was achieved by continuous infusion of a reference mass solution, which enabled accurate mass spectral measurements with an error of less than 5 parts-per-million (ppm).

Kinetic measurements

L-Alanine dehydrogenase (LADH) assays.—Alr activity was monitored continuously at 37 °C by UV-Vis spectrophotometry (Shimadzu UV-2550, Milton Keynes, UK) using a 1 cm path-length cell and coupling D-Ala to L-Ala conversion to reduction of NAD+ to NADH via an LADH system[20]. The *E. coli* orthologue of LADH, AlaA, used for the assay was co-expressed as His-tagged protein with pGro7 plasmid (Takara Bio, Cat.# 3340) and purified by Ni affinity chromatography. Gel filtration was performed after cleavage of the His-tag by thrombin using a 26/60 Sephadex column.

Reaction mixture for inactivation kinetics experiments (Fig. 1e) contained 50 mM TAPS (pH 8.2), 100 mM KCl, 1 mM NAD$^+$, 50 μL/mL of LADH stock (550 U/mL), 0.02 μM MtAlr, 10 mM D-Ala, and variable DCS concentration (0.1, 0.25, 1, 2, 5 mM).

Reaction mixture for initial velocities of MtAlr activity as a function of DCS concentration (Fig. 1f) contained 100 mM potassium phosphate (pH 8.0), 1 mM NAD$^+$, 50 μL/mL of LADH stock (550 U/mL), 0.2 μM MtAlr, 10 mM D-Ala, and variable DCS concentration (0, 25, 50, 75, 100, 125 μM).

Enzyme activity monitored by CD—Residual activity of MtAlr after DCS inactivation and removal of unbound DCS (Fig. 2a, inset) was monitored by circular dichroism at 37 °C using a Jasco-715 spectropolarimeter and a 2 mm pathlength cuvette. Activity was measured

following racemization of L-Ala through change of dichroic signal at 205 nm. Reaction was started by addition of L-Ala, to a final concentration of 5 mM, to a sample containing 0.8 μM MtAlr in 50 mM sodium phosphate (pH 7.5), 100 mM KCl. Samples treated with PLP were preliminarily incubated with 4 μM PLP at 37 ° C for 2 h.

Racemization kinetics of L-Ala and DCS by MtAlr (Fig. 2e)at 37 °C were checked monitoring CD signal at 205 nm and 230 nm, respectively. Concentrations were 1.5 μM MtAlr, L-Ala 5 mM and DCS 2.5 mM in 20 mM sodium phosphate (pH 7.5).

Fluorescence and UV/Visible spectroscopy

Fluorescence spectra were acquired using a Shimadzu Fluorometer RF5301 and a 0.5 x 1 cm path-length cell for absorbed and emitted light. The temperature was kept at 37 °C using a circulating water bath. Slit widths were 1.5/3 nm for intrinsic tryptophan fluorescence (λmax excitation 284 nm/emission 327 nm), 1.5/10 nm for isoxazole (λmax 318 nm/357 nm), 1.5/20 nm for oxime (λmax 365 nm/454 nm), and 5/15 nm for aldimine (λmax 434 nm/520 nm). Protein concentration was in the range 2.5-5 μM in 50 mM sodium phosphate pH 7.5, 100 mM KCl. The occurrence of internal quenching under these conditions has been preliminarily checked and excluded. Spectra were corrected for buffer contribution.

UV/Visible absorbance spectra were acquired at 37 °C using a Shimadzu UV-2550 spectrophotometer (Milton Keynes, UK) equipped with a thermostatic cell holder and using a 1 cm path-length cell.

DCS Inhibition, Crystallisation and X-ray data collection

MtAlr was preliminarily inactivated by DCS over 1 h at 30 °C (MtAlr:DCS ratio 1:100) and then kept at 20 °C until drops were set up 24 h later.

Crystals of DCS-inhibited MtAlr were grown at 20 °C from sitting drops of 0.2 μL formed by 0.1 μL inhibited enzyme stock solution (20 mg/ml in 20 mM Tris pH 7.0) and 0.1 μL crystallisation solution containing: 100 mM sodium MES buffer pH 6.2, 150 mM CaCl, 10% (v/v) PEG Smear Broad (Molecular Dimensions), 3% (v/v) Glycerol. Cryoprotection was provided by preparing a 3:1 mixture of the crystallisation condition with 100% Glycerol. The crystals were transferred into this cryoprotectant prior to freezing in liquid nitrogen for data collection. Diffraction data were collected at beamline I04-1 at the Diamond Light Source, U.K. Integration and scaling were performed using DIALS within the XIA2 expert system for X-ray diffraction data processing[36]. Crystals belong to the tetragonal space group $P4_12_12$ with two molecules in the crystallographic asymmetric unit.

Structure determination and refinement

Molecular replacement was carried out with PHASER[37], using the coordinates of *M. tuberculosis* alanine racemase (PDB code 1XFC) with ligands and solvent molecules removed. Models were improved and refined using COOT[38] and PHENIX[39]. A summary of the data collection and refinement statistics is given in Supplementary Table 1. The Ramachandran plot showed 97.3% and 2.7% of residues in the most favoured and in allowed

regions, respectively. Figures were drawn using PyMol (The PyMol Molecular Graphics System, Version 2.0 Schrödinger, LLC).

Molecular replacement was carried out with PHASER[37], using the coordinates of *M. tuberculosis* alanine racemase (PDB code 1XFC) with ligands and solvent molecules removed. Models were improved and refined using COOT[38] and PHENIX[39]. A summary of the data collection and refinement statistics is given in Supplementary Table 1. The Ramachandran plot showed 97.3% and 2.7% of residues in the most favoured and in allowed regions, respectively. Figures were drawn using PyMol (The PyMol Molecular Graphics System, Version 2.0 Schrödinger, LLC).

NMR spectroscopy

The NMR measurements were performed either at 25 or 37 °C, on Bruker spectrometers operating at 400 MHz, 600 MHz, 700 MHz, 800 MHz and 950 MHz and equipped with 5 mm TCI cryoprobes or with a broadband SmartProbe (400 MHz) as detailed in figure captions of each spectrum. ^{1}H-NMR spectra were recorded using either a 1D NOESY sequence or a 1D sequence with presaturation. Spectra were processed and analysed using Bruker TopSpin3.6 or MestReNova 12.

H/D exchange experiments—1D ^{1}H and 1D ^{13}C (data not shown) spectra for the H/D exchange experiment were acquired on a sample containing 0.6 μM MtAlr in 20 mM sodium phosphate buffer (pH 7.5), 80 mM KCl, 5 mM DCS. The sample was incubated at 37 °C for 5 h prior to spectra acquisition.

Oxime assignment—For the assignment of the oxime in the model system, PLP and DCS were combined at 50 mM in a 1:1 ratio in 50 mM potassium phosphate in D_2O (pD 6.9) and allowed to react for 6 h at room temperature until no further change of pD was observed. Adjustment of pD to the final value was done before 1D ^{1}H and 2D ^{1}H^{15}N- HMBC and 2D ^{1}H^{13}C-HSQC spectra at natural abundance of ^{13}C and ^{15}N were acquired. To confirm the formation of a linear oxime, 10 mM PLP and 10 mM DCS were combined in 50 mM potassium phosphate (pH 7.3) in either 100% $H_2^{16}O$ or $H_2^{16}O$:$H_2^{18}O$ (1:1) and allowed to react at room temperature for 6 h until no further change of pH was observed. Adjustment of pH to final value was done prior to acquisition of 1D ^{1}H and ^{13}C spectra acquisition.

Synthetic isoxazole tautomerism—1D ^{1}H and 1D ^{13}C (data not shown) spectra for the characterisation of isoxazole tautomerism were acquired on a sample containing 2 mM isoxazole in 50 mM sodium phosphate (pH 7.5), 100 mM KCl, either in D_2O or H_2O.

Synthesis of the fully aromatized isoxazole

(4-(((3-hydroxyisoxazol-4-yl)ammonio)methyl)-6-methyl-5-oxidopyridin-3-yl)methyl phosphate **6** Pyridoxal 5'-phosphate **7** (211.6 mg, 0.79 mmol) and D-cycloserine **3** (80.5 mg, 0.79 mmol, 1 eq.) were suspended in methanol containing 5% H_2O (8 mL). The bright yellow mixture was then stirred while heating to 50 °C for 16 h. The precipitate that formed was isolated by filtration to obtain a light yellow powder which was purified by reverse phase chromatography (gradient elution, 0-10% $(NH_4)HCO_3$ buffer/acetonitrile). The

product was dried by lyophilisation, yielding the product **6** as a yellow powder (121.5 mg, 0.37 mmol, 47%).

^{1}H NMR (400 MHz, D_2O) • 7.75 (s, 1H, Pyr-*H*), 7.72 (s, 1H, N-O-C*H*-C), 4.83 (d, [3]J_{P-H} = 6.2 Hz, 2H, Pyr-C*H*$_2$-O-P), 4.23 (s, 2H, Pyr-C*H*$_2$-NH), 2.37 (s, 3H, Pyr-C*H*$_3$); ^{13}C NMR (101 MHz, D_2O) • 171.07, 157.64, 144.07, 143.80, 136.92, 133.55, 133.47, 128.36, 121.71, 61.66 (d, [2]J_{C-P} = 4.2 Hz), 43.86, 15.38; HRMS (ESI+): *m/z* calculated for $C_{11}H_{15}N_3O_7P$ (M +H^{+}): 332.0642, found 332.0637, -3.07 ppm; R_f = 7.743 min (85%-10% pH 9 NH_4OAc/ ACN, Waters X-bridge Amide HILIC column).

Supplementary Material

Refer to Web version on PubMed Central for supplementary material.

Acknowledgements

References

1. Harris DA, et al. Discovery, development, and antimicrobial properties of D-4-amino-3-isoxazolidone (oxamycin), a new antibiotic produced by Streptomyces garyphalus n. sp. Antibiot Chemother (Northfield). 1955; 5:183–90. [PubMed: 24543464]

2. Caminero JA, Sotgiu G, Zumla A, Migliori GB. Best drug treatment for multidrug-resistant and extensively drug-resistant tuberculosis. Lancet Infect Dis. 2010; 10:621–9. [PubMed: 20797644]

3. Walsh CT. Enzymes in the D-alanine branch of bacterial cell wall peptidoglycan assembly. J Biol Chem. 1989; 264:2393–6. [PubMed: 2644260]

4. Batson S, et al. Inhibition of D-Ala:D-Ala ligase through a phosphorylated form of the antibiotic D-cycloserine. Nat Commun. 2017; 8:1939. [PubMed: 29208891]

5. Mullins LS, Zawadzke LE, Walsh CT, Raushel FM. Kinetic evidence for the formation of D-alanyl phosphate in the mechanism of D-alanyl-D-alanine ligase. J Biol Chem. 1990; 265:8993–8. [PubMed: 2188969]

6. Fenn TD, Stamper GF, Morollo AA, Ringe D. A side reaction of alanine racemase: transamination of cycloserine. Biochemistry. 2003; 42:5775–83. [PubMed: 12741835]

7. Olson GT, Fu M, Lau S, Rinehart KL, Silverman RB. An Aromatization Mechanism of Inactivation of γ-Aminobutyric Acid Aminotransferase for the Antibiotic l-Cycloserine. Journal of the American Chemical Society. 1998; 120:2256–2267.

8. Peisach D, Chipman DM, Van Ophem PW, Manning JM, Ringe D. d-Cycloserine Inactivation of d-Amino Acid Aminotransferase Leads to a Stable Noncovalent Protein Complex with an Aromatic Cycloserine-PLP Derivative. Journal of the American Chemical Society. 1998; 120:2268–2274.

9. Noda M, Matoba Y, Kumagai T, Sugiyama M. Structural evidence that alanine racemase from a D-cycloserine-producing microorganism exhibits resistance to its own product. J Biol Chem. 2004; 279:46153–61. [PubMed: 15302886]

10. Wu D, et al. Residues Asp164 and Glu165 at the substrate entryway function potently in substrate orientation of alanine racemase from E. coli: Enzymatic characterization with crystal structure analysis. Protein Sci. 2008; 17:1066–76. [PubMed: 18434499]

11. Priyadarshi A, et al. Structural insights into the alanine racemase from Enterococcus faecalis. Biochim Biophys Acta. 2009; 1794:1030–40. [PubMed: 19328247]

12. Asojo OA, et al. Structural and biochemical analyses of alanine racemase from the multidrug-resistant Clostridium difficile strain 630. Acta Crystallogr D Biol Crystallogr. 2014; 70:1922–33. [PubMed: 25004969]

13. Tassoni R, van der Aart LT, Ubbink M, van Wezel GP, Pannu NS. Structural and functional characterization of the alanine racemase from Streptomyces coelicolor A3(2). Biochem Biophys Res Commun. 2017; 483:122–128. [PubMed: 28042035]

14. LeMagueres P, et al. The 1.9 A crystal structure of alanine racemase from Mycobacterium tuberculosis contains a conserved entryway into the active site. Biochemistry. 2005; 44:1471–81. [PubMed: 15683232]

15. Prosser GA, de Carvalho LP. Metabolomics Reveal d-Alanine:d-Alanine Ligase As the Target of d-Cycloserine in Mycobacterium tuberculosis. ACS Med Chem Lett. 2013; 4:1233–1237. [PubMed: 24478820]

16. Halouska S, et al. Metabolomics analysis identifies d-Alanine-d-Alanine ligase as the primary lethal target of d-Cycloserine in mycobacteria. J Proteome Res. 2014; 13:1065–76. [PubMed: 24303782]

17. Evangelopoulos D, et al. Comparative fitness analysis of D-cycloserine resistant mutants reveals both fitness-neutral and high-fitness cost genotypes. Nat Commun. 2019; 10:4177. [PubMed: 31519879]

18. Copeland, RA. Evaluation of enzyme inhibitors in drug discovery : a guide for medicinal chemists and pharmacologists. John Wiley, Hoboken NJ; Chichester: 2005.

19. Kurokawa Y, Watanabe A, Yoshimura T, Esaki N, Soda K. Transamination as a side-reaction catalyzed by alanine racemase of Bacillus stearothermophilus. J Biochem. 1998; 124:1163–9. [PubMed: 9832621]

20. Wang E, Walsh C. Suicide substrates for the alanine racemase of Escherichia coli B. Biochemistry. 1978; 17:1313–21. [PubMed: 350267]

21. Noda M, et al. Self-protection mechanism in D-cycloserine-producing Streptomyces lavendulae. Gene cloning, characterization, and kinetics of its alanine racemase and D-alanyl-D-alanine ligase, which are target enzymes of D-cycloserine. J Biol Chem. 2004; 279:46143–52. [PubMed: 15302885]

22. Ahmed SA, Esaki N, Tanaka H, Soda K. Mechanism of alpha-amino-epsilon-caprolactam racemase reaction. Biochemistry. 1986; 25:385–8. [PubMed: 3955003]

23. Churchich JE. Fluorescence properties of pyridoxamine 5-phosphate. Biochim Biophys Acta. 1965; 102:280–8. [PubMed: 5833405]

24. Churchich JE, Farrelly JG. Mechanism of binding of pyridoxamine 5-phosphate to the apoenzyme aspartate aminotransferase. Fluorescence studies. J Biol Chem. 1969; 244:3685–90. [PubMed: 5794234]

25. Bridges JW, Davies DS, Williams RT. Fluorescence studies on some hydroxypyridines including compounds of the vitamin B6 group. Biochem J. 1966; 98:451–68. [PubMed: 5941339]

26. Bueno C, Encinas MV. Photophysical and Photochemical Studies of Pyridoxamine. Helvetica Chimica Acta. 2003; 86:3363–3375.

27. Chan-Huot M, et al. NMR studies of protonation and hydrogen bond states of internal aldimines of pyridoxal 5'-phosphate acid-base in alanine racemase, aspartate aminotransferase, and poly-L-lysine. J Am Chem Soc. 2013; 135:18160–75. [PubMed: 24147985]

28. Khomutov, RM; Karpeisky, MYA; Severin, ES. The predetermined synthesis of inhibitors for pyridoxalic enzymes. Chemical and biological aspects of pyridoxal catalysis : proceedings of a symposium of the International Union of Biochemistry; Rome. October 1962; Oxford: Pergamon, Symposium Publications Division; 1963. 313–321.

29. Feng Z, Barletta RG. Roles of Mycobacterium smegmatis D-alanine:D-alanine ligase and D-alanine racemase in the mechanisms of action of and resistance to the peptidoglycan inhibitor D-cycloserine. Antimicrob Agents Chemother. 2003; 47:283–91. [PubMed: 12499203]

30. Churchich JE. The interaction of cycloserine with glutamate aspartate transaminase as measured by fluorescence spectroscopy. J Biol Chem. 1967; 242:4414–7. [PubMed: 6065087]

31. Ju J, et al. Correlation between catalytic activity and monomer-dimer equilibrium of bacterial alanine racemases. J Biochem. 2011; 149:83–9. [PubMed: 20971724]

32. Strych U, Benedik MJ. Mutant analysis shows that alanine racemases from Pseudomonas aeruginosa and Escherichia coli are dimeric. J Bacteriol. 2002; 184:4321–5. [PubMed: 12107154]

33. Ondrechen MJ, Briggs JM, McCammon JA. A model for enzyme-substrate interaction in alanine racemase. J Am Chem Soc. 2001; 123:2830–4. [PubMed: 11456969]

34. Batt SM, et al. Structural basis of inhibition of Mycobacterium tuberculosis DprE1 by benzothiazinone inhibitors. Proc Natl Acad Sci U S A. 2012; 109:11354–9. [PubMed: 22733761]

35. Prosser GA, et al. Glutamate Racemase Is the Primary Target of beta-Chloro-d-Alanine in Mycobacterium tuberculosis. Antimicrob Agents Chemother. 2016; 60:6091–9. [PubMed: 27480853]

36. Winter G. xia2: an expert system for macromolecular crystallography data reduction. Journal of Applied Crystallography. 2010; 43:186–190.

37. McCoy AJ, et al. Phaser crystallographic software. Journal of Applied Crystallography. 2007; 40:658–674. [PubMed: 19461840]

38. Emsley P, Cowtan K. Coot: model-building tools for molecular graphics. Acta Crystallogr D Biol Crystallogr. 2004; 60:2126–32. [PubMed: 15572765]

39. Afonine PV, et al. Towards automated crystallographic structure refinement with phenix.refine. Acta Crystallographica Section D. 2012; 68:352–367.
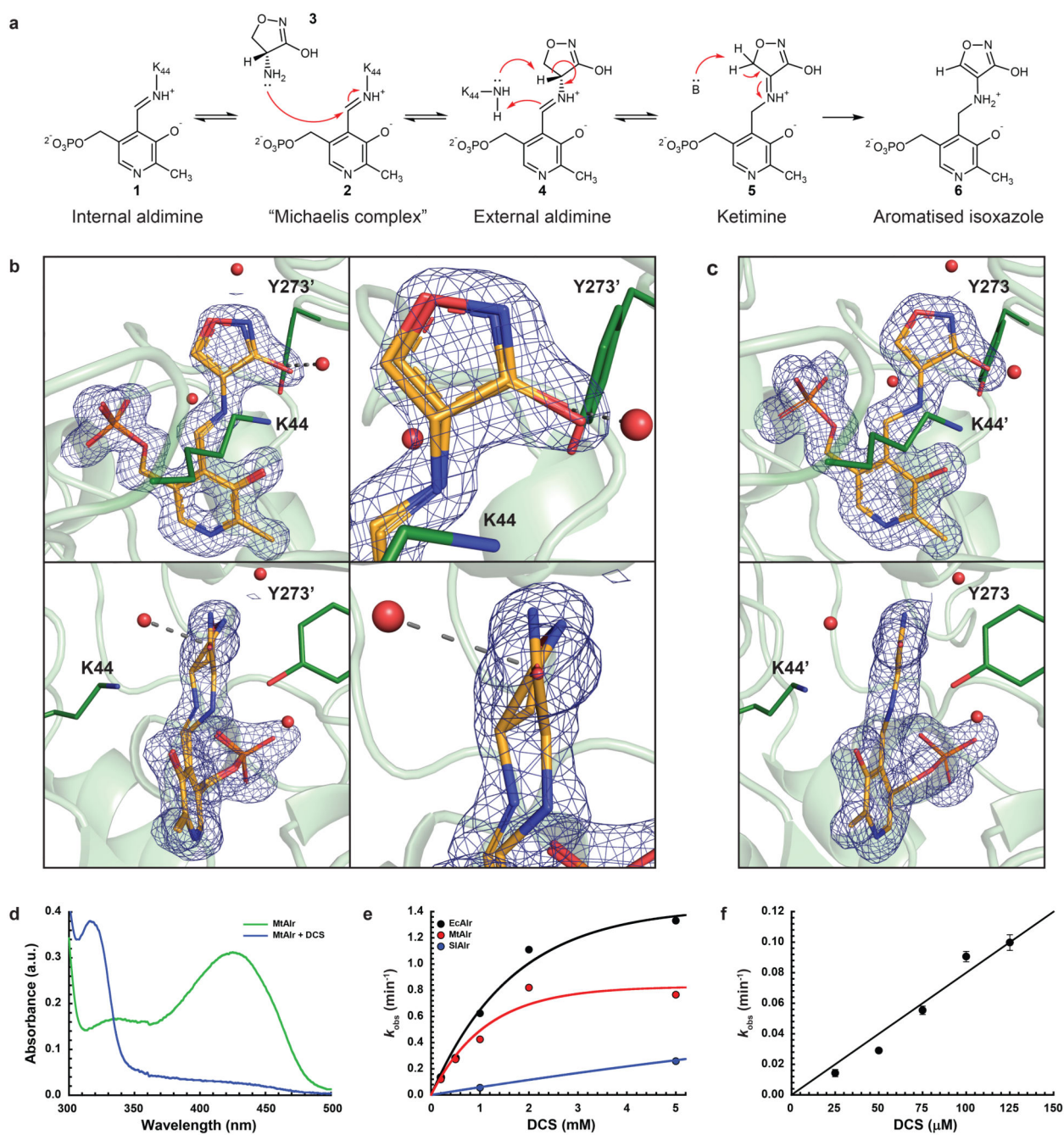
**Figure 1. Currently proposed mechanism and experimental data in support of irreversible inhibition.**

a, Scheme of current model for the inactivation mechanism of alanine racemase (Alr) by DCS, assuming that isoxazole **6** is formed irreversibly[6]. **b,c,** Crystal structure of MtAlr inhibited with DCS, showing external aldimine **4** and isoxazole **6** in site A (**b**), and isoxazole in site B (**c**) in a front (top) and ~90° rotated (around Y axis) view (bottom). 2Fo-Fc difference electron map of the enzymatic products in each site is represented at 1 r.m.s.d.. Sidechains of catalytic residues Lys44 and Tyr273' are shown in dark green. Three

conserved water molecules within a distance of 5 Å of the DCS carbonyl of the aldimine **4** are shown as red spheres. The hydrogen bond of a water to the carbonyl oxygen of the aldimine is shown as a dashed line. **d**, UV-visible spectrum of (active) MtAlr showing the internal aldimine absorbance at 434 nm (green) and DCS-inhibited MtAlr showing the putative absorbance of isoxazole and/or ketimine at 318 nm (blue). **e**, Inactivation rates (k_{obs}) for Alrs. **f**, Zoom-in on the MtAlr inactivation kinetics at low DCS concentrations illustrating the intercept at 0, suggesting irreversibility.
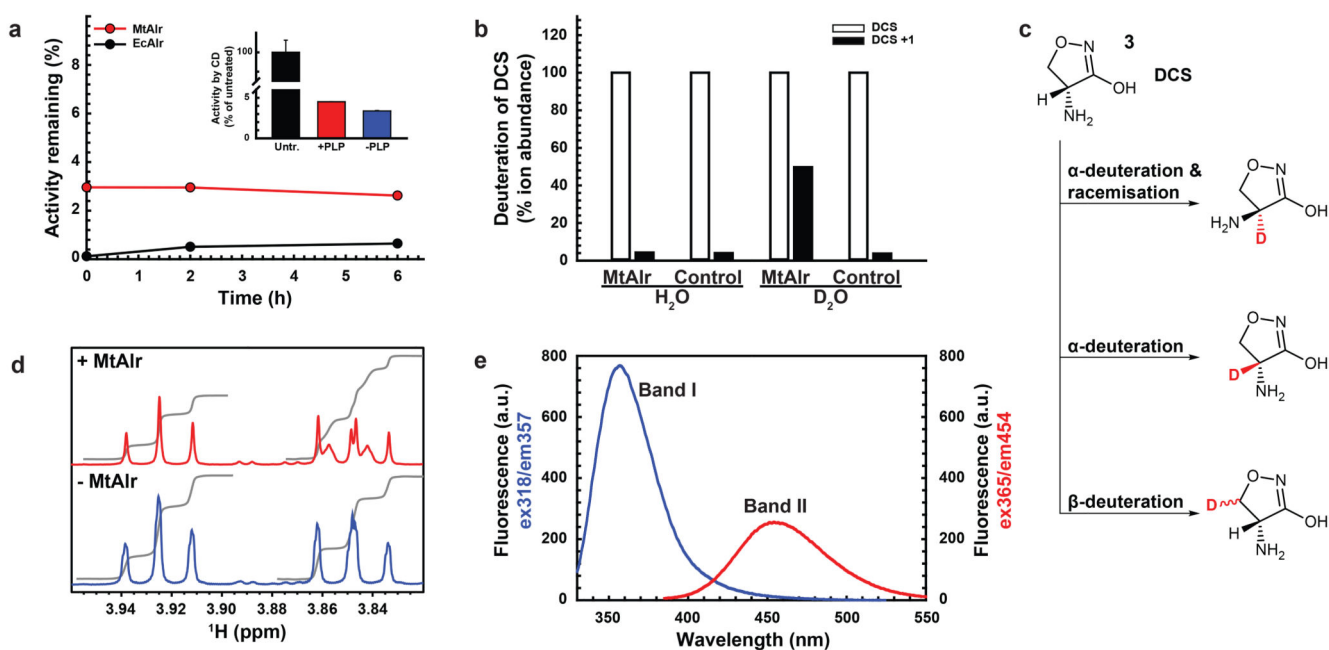
Figure 2. New experimental evidence suggesting a more complex inhibition mechanism.
a, MtAlr and EcAlr residual activity, detected after DCS inhibition and removal of excess DCS, as measured by LADH enzymatic assay and by CD (inset). CD data compare samples of inhibited MtAlr treated or not treated with additional PLP after DCS elimination by filtration. **b**, Deuterium incorporation in DCS as measured by LC-MS. **c**, Possible sites of deuterium incorporation in DCS. **d**, 1D ^{1}H-NMR spectrum (600 MHz) of DCS in D_2O showing signals for the α (3.935 ppm) and one β (3.855 ppm) proton in the absence and presence of MtAlr. Upon incubation with MtAlr, the α proton signal integral decreases by 35%, indicating that such a fraction has been replaced with deuterium, while the region corresponding to the β proton exhibits a new doublet resonance arising from the deuterated species, which lacks $^{3}J_{αβ}$ coupling as well as showing a small isotope shift. **e**, Two distinct products of the inactivation reaction are detected by fluorescence. The compound giving rise to band I, putatively isoxazole **6** (Fig. 1a) can be separated from the additional unknown compound (band II) by filtration (Supplementary Fig. 2k).
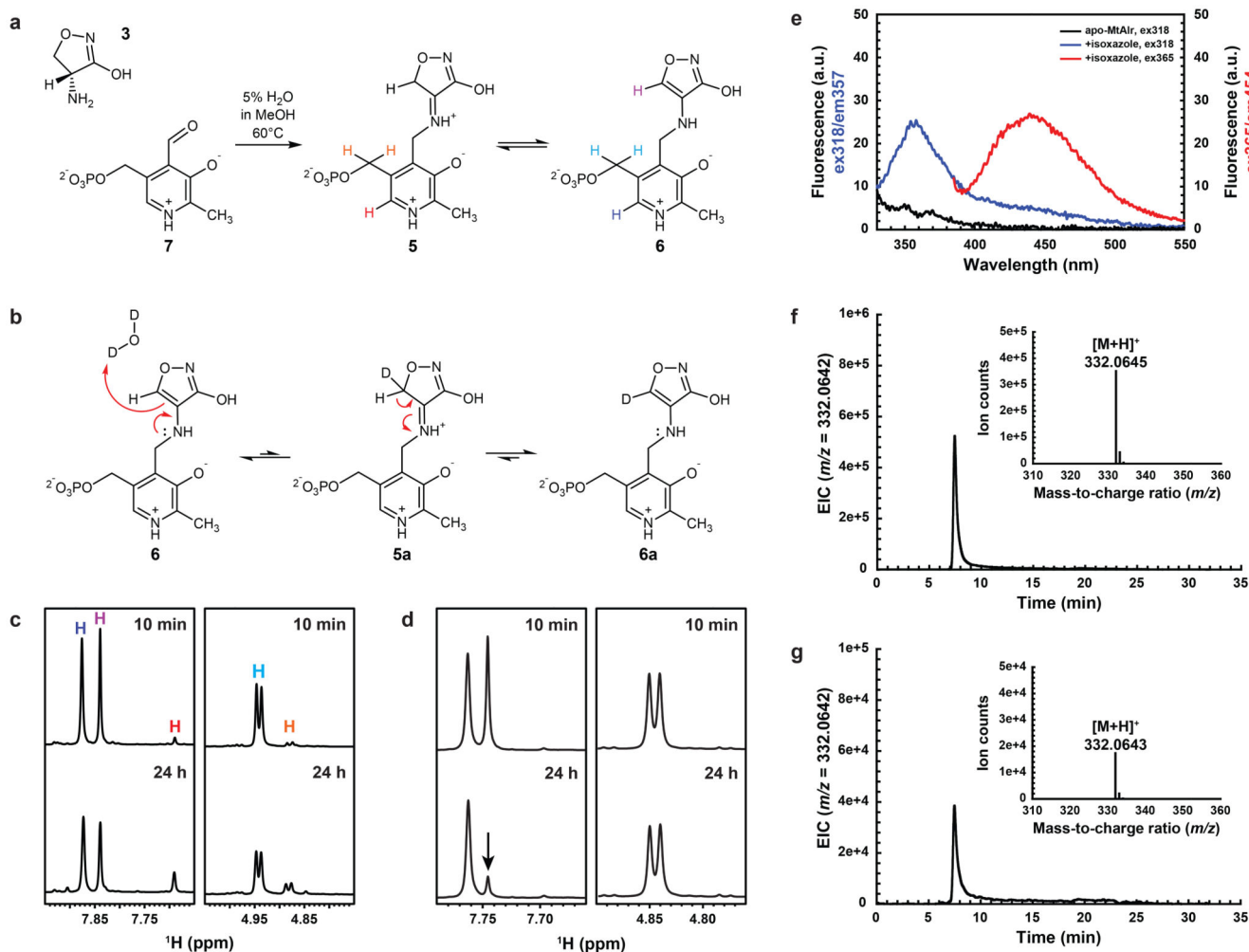
Figure 3. Chemical synthesis of the isoxazole adduct 6 reveals tautomerism in aqueous solution.
a, Isoxazole (**6**) synthetic scheme. **b**, Mechanism of isoxazole/ketimine tautomerism. When the reaction takes place in deuterated solution, replacement of the isoxazole **6** proton with deuterium is observed. **c**, 1D ^{1}H-NMR spectrum (600 MHz) of the isoxazole at 37 °C in aqueous solution shows a decrease in isoxazole **6** protons (light, dark blue, and purple) (Fig. 3a) and an increase in ketimine **5** protons (orange and red) (Fig. 3a) indicative of conversion of isoxazole **6** into ketimine **5** up to 20% in 24 h. **d**, 1D ^{1}H-NMR spectrum (600 MHz) of the isoxazole at 25 °C in buffered deuterated solution shows a substantial decrease in the isoxazole **6** proton signal upon deuterium substitution (arrow) without appreciable increase in the ketimine content, which is observed when the experiment is performed at 37 °C. **e**, Apo-MtAlr incubated with the synthetic isoxazole **6** to reconstitute the inhibited enzyme species, showing the resulting isoxazole **6** and substituted oxime **11** bands (see Fig. 4b). **f,g**, Extracted ion chromatograms for *m/z* 332.0642, showing the retention time and mass spectra (inset) for the isoxazole **6** formed synthetically (**f**) and enzymatically (**g**).
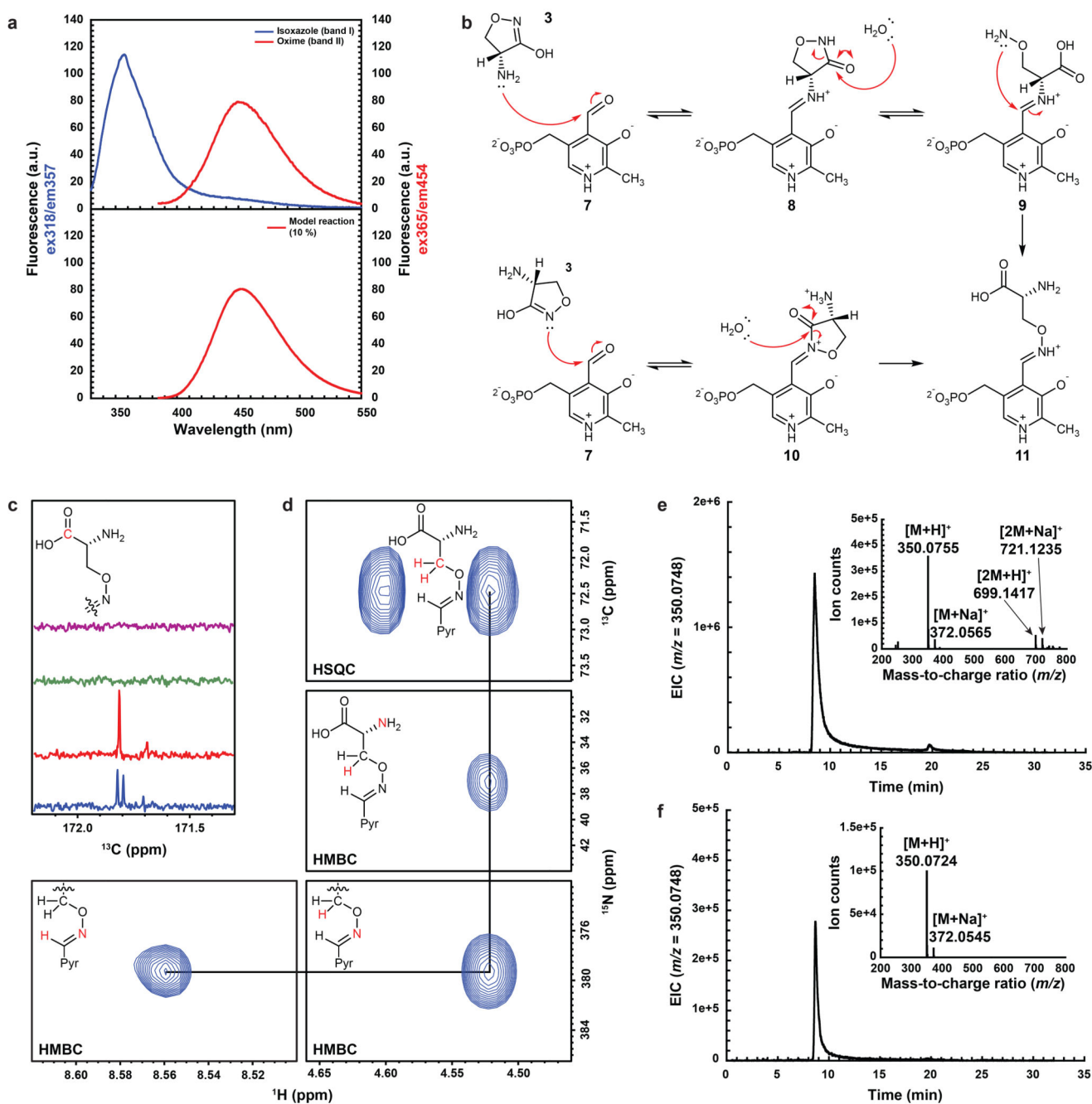
Figure 4. Assignment of the second fluorescent product of the inactivation.
a, Comparison between fluorescent species as products of the enzymatic inactivation reaction (top) and model reaction between PLP and DCS in buffer (bottom). In the model reaction the PLP concentration was equal to the MtAlr concentration of the enzymatic reaction. The signal of enzymatic reaction band II is equal in intensity to 10% of the model reaction indicating that 10% of PLP from the enzymatic reaction contributes to the substituted oxime formation upon reaction with DCS. **b**, Reaction scheme showing the two theoretical possibilities for substituted oxime formation from PLP and DCS in a model

reaction. Although the reactivity of the ring nitrogen is expected to be substantially lower than that of the primary amine and would make **10** unlikely to form, we considered both for completeness. **c**, 1D ^{13}C spectra (700 MHz) of the carbonyl region for the product of the substituted oxime model reaction in a $H_2{}^{16}O$ (red) and $H_2{}^{16}O$:$H_2{}^{18}O$ (1:1) buffer solution (blue). The substituted oxime carbonyl signal is split in the $H_2{}^{16}O$:$H_2{}^{18}O$ spectrum as a consequence of the $H_2{}^{18}O$ isotope effect, indicating that hydrolysis of the DCS ring has occurred in the product. DCS controls in $H_2{}^{16}O$ (purple) and $H_2{}^{16}O$:$H_2{}^{18}O$ (1:1) buffer solution (green) confirm that the observed carbonyl does not arise from hydrolysis of unreacted DCS. **d**, Assignment of model substituted oxime by 2D NMR: $^1H^{15}N$ –HMBC, $^1H^{13}C$–HSQC (950 MHz). Pairs of correlating atoms in spectra are highlighted in red. In the $^1H^{15}N$–HMBC spectrum, a $^3J_{HN}$ through bond correlation is observed between the β proton at 4.52 ppm (assigned in the HSQC) and two nitrogen atoms with chemical shifts typical of an amine (37 ppm) and a substituted oxime (379 ppm). The oxime nitrogen, as expected, further correlates with the substituted oxime proton at 8.56 ppm. This correlation pattern is consistent with either a cyclic **10** or linear oxime **11**. The carbonyl split observed in Fig. 4c (blue) confirms that the substituted oxime is linear **11**. **e**, **f**, Extracted ion chromatogram for *m/z* 350.0748 showing the retention time and mass spectra (inset) for the substituted oxime **11** formed in the model reaction (**e**) and in the enzymatic reaction (**f**).
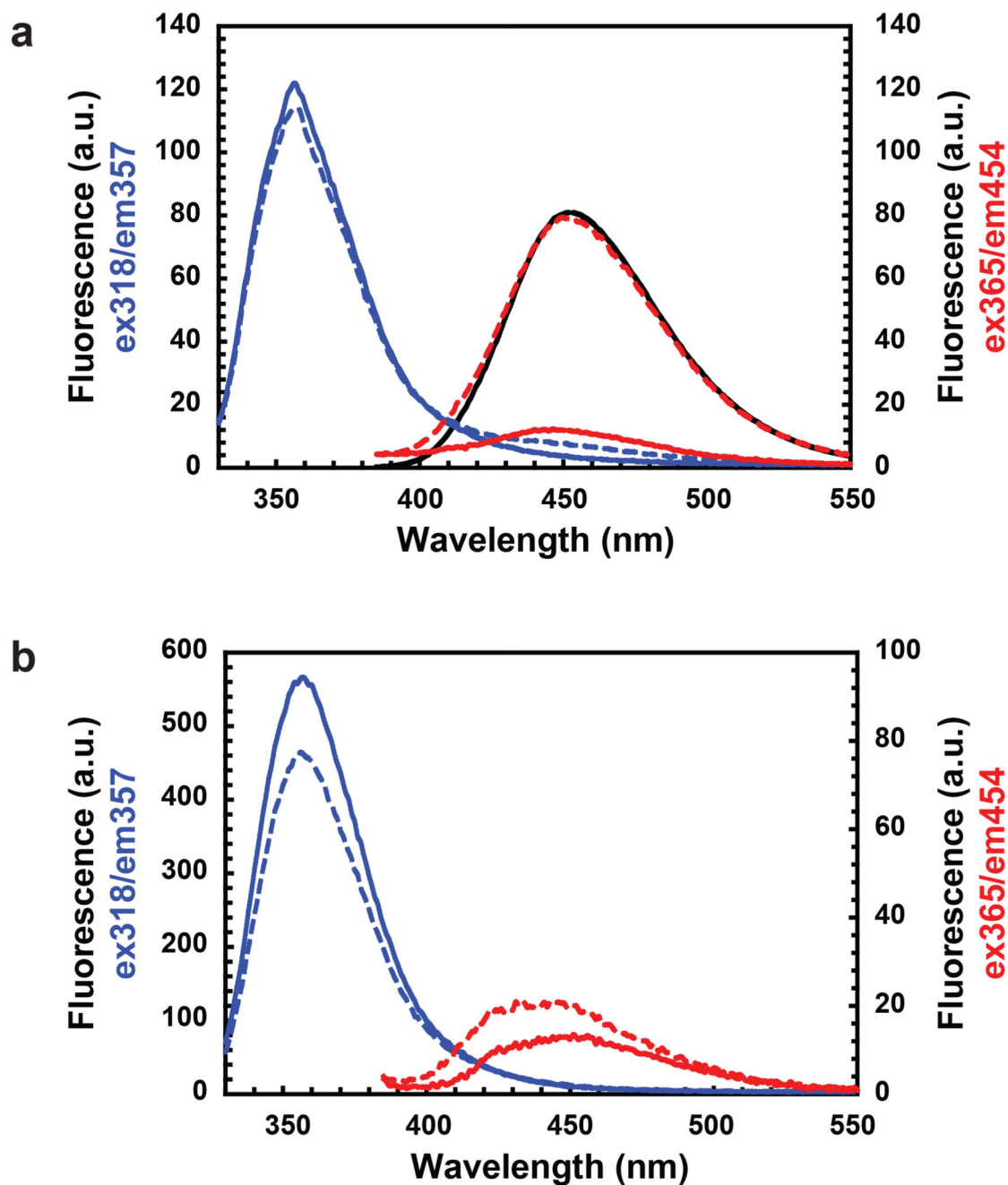
Figure 5. The isoxazole adduct is not a stable irreversible inhibitor of Alr.
a, Fluorescence emission spectra of isoxazole **6** and substituted oxime **11** from the enzymatic reaction, showing the difference in signal intensity at 2 h (solid lines) compared to the signal intensity at 24 h when substituted oxime reaches a plateau (dotted lines). The signal of the substituted oxime **11** from enzymatic reaction at 24 h is equal in intensity to 10% of the model reaction (black solid line) indicating that 10% of PLP from the enzymatic reaction contributes to the substituted oxime formation upon reaction with DCS. **b,** Fluorescence emission spectra of isoxazole **6** and substituted oxime **11** immediately after

ultrafiltration, performed after 24 h inhibition with DCS (solid lines) and after 24 h of further incubation at 37 °C (dotted lines), showing the decrease in intensity of the isoxazole **6** signal and the corresponding increase of the substituted oxime **11** signal.
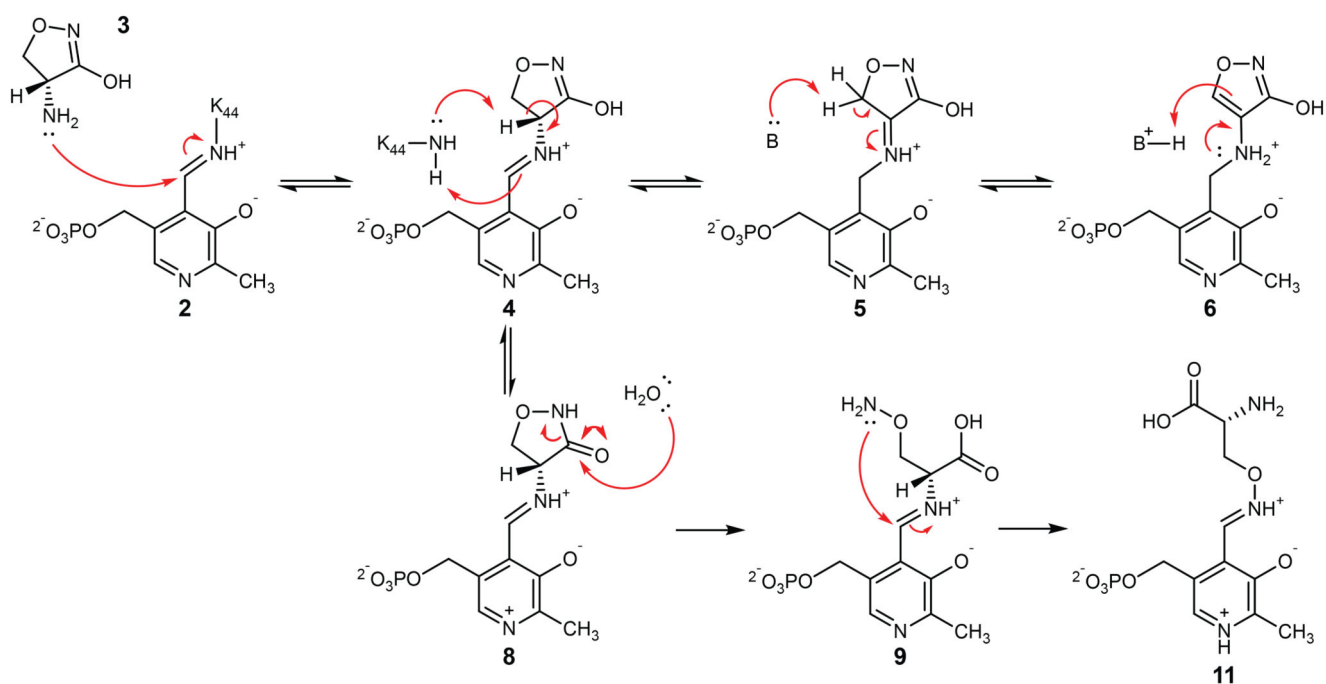
Figure 6. Revised complete mechanism of DCS inactivation of alanine racemases.
The revised mechanism shows the formation of a second product in the form of a linear
substituted oxime **11** which is released into solution. This irreversible "oxime-forming
pathway" runs alongside the "isoxazole-forming pathway" which has been proven to be
reversible at all steps from **2** to **6**.